Preparation and Structure of the Ion-Conducting Mixed Molecular Glass Ga$_2$I$_{3.17}$

Alfred Amon,* M. Emre Sener, Alexander Rosu-Finsen, Alex C. Hannon, Ben Slater, and Christoph G. Salzmann

Read Online

ACCESS | Metrics & More | Article Recommendations | Supporting Information

ABSTRACT: Modern functional glasses have been prepared from a wide range of precursors, combining the benefits of their isotropic disordered structures with the innate functional behavior of their atomic or molecular building blocks. The enhanced ionic conductivity of glasses compared to their crystalline counterparts has attracted considerable interest for their use in solid-state batteries. In this study, we have prepared the mixed molecular glass Ga$_2$I$_{3.17}$ and investigated the correlations between the local structure, thermal properties, and ionic conductivity. The novel glass displays a glass transition at 60 °C, and its molecular make-up consists of GaI$_4^-$ tetrahedra, Ga$_2$I$_6^{2-}$ heteroethane ions, and Ga$^+$ cations. Neutron diffraction was employed to characterize the local structure and coordination geometries within the glass. Raman spectroscopy revealed a strongly localized nonmolecular mode in glassy Ga$_2$I$_{3.17}$, coinciding with the observation of two relaxation mechanisms below T_g in the AC admittance spectra.
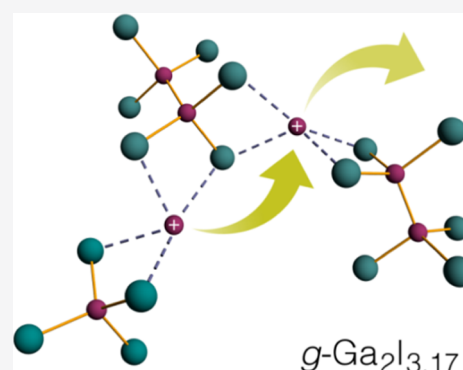
INTRODUCTION

Glasses belong to the earliest materials utilized and produced by humanity and have been rediscovered as modern materials based on diverse novel glass-forming precursors and the concomitant functional properties.[1] Recent examples are flexible semiconducting oxide glasses,[2] multinary chalcogenide glasses for infrared optics and data-storage media,[3] bulk metallic glasses with superior mechanical and magnetic properties,[4] and metal−organic framework glasses.[5,6] Ion-conducting glasses are promising electrolytes for the next-generation of all-solid-state batteries, as they display isotropic behavior, absence of grain boundaries, and often higher ionic conductivity than their ordered crystalline counterparts.[7] In addition to amorphous organic polymers, mixed phosphate, oxide, sulfide, and halide glasses show high ionic conductivities at ambient temperature, combined with enhanced chemical stability and glass-forming ability.[8−10]

Molecular glasses are typically comprised of small organic molecules[11,12] and have been investigated for applications in photolithography, organic electronics,[13−15] and for amorphous pharmaceuticals where their improved dissolution behavior can be exploited.[16,17] The small molecular mass and well-defined composition make molecular glasses attractive for the production of printed organic circuits.[18] However, low glass-transition temperatures T_g and strong tendencies for crystallization remain the major challenges in the design of molecular glasses and hinder long-term applications, in particular, at elevated temperatures.[19]

The general design guidelines for molecular glasses include nonplanar molecular structures, increased molecular size, and bulky substituents,[13] as observed in a series of molecular glasses, based on triphenylamine derivatives, tris-(oligoarylenyl)amines or tris(oligoarylenyl)boranes.[20,21] Tuning the glass-transition temperature, long-term stability, and optical and transport properties has been achieved by side-group substitution and variation in molecular size but still relies often on trial-and-error.[11,22] More recent avenues to molecular glass design include the use of atomistic simulations or machine-learning-based algorithms to predict the properties and compositions of possible glass-forming liquids.[12,23,24] For organic electronics, interest has shifted from one-component glasses to mixed molecular glasses, containing two or more molecular species.[25] For applications such as organic LEDs, the combination of light-emitting species with conductive molecules can lead to increased emission efficiency and provides more design flexibility.[26]

Contrary to the glass-forming organic liquids, inorganic oxide, chalcogenide, or halide glasses typically feature a network structure, characterized by the formation of strong directional bonds during the transition from the liquid to the
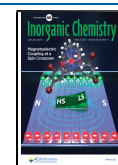
glassy state.[27] The presence of individual molecular units has been reported in a few chalcogenide glasses, notably PS_4^{3-} and $P_2S_6^{4-}$ in ion-conducting glasses,[10,28,29] P_4Se_n (n = 3−4) in nonstoichiometric P−Se glasses,[30,31] As_4S_4 molecules in As−S glasses,[32] as well as the analogous multinary P−As−S−Se species.[33] Of special interest is the typically elevated glass-transition temperature (T_g > 100 °C) in inorganic molecular glasses compared to organic glass-forming liquids.[11,25,33]

For the gallium−iodine system, the crystalline binary compounds Ga_2I_6, Ga_2I_4, and Ga_2I_3 have been reported (cf. Figure 1A).[34−36] The latter two are crystalline salts comprised
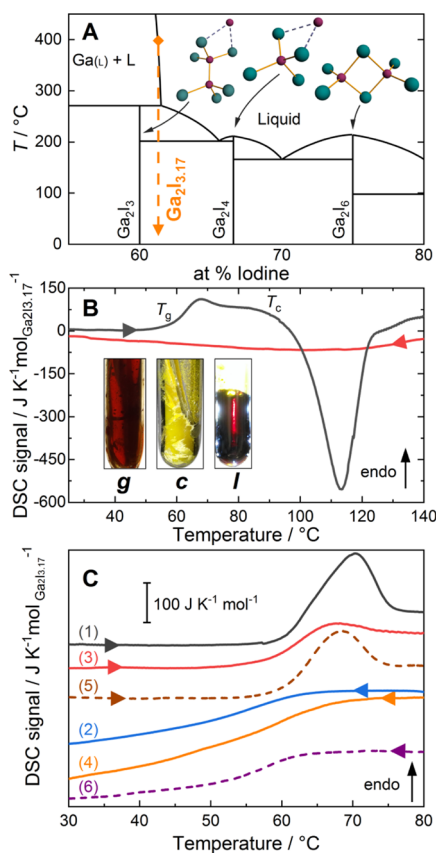

Figure 1. (A) Partial phase diagram of the gallium−iodine system adapted from refs 37 and 42. Molecular entities in the crystalline compounds are sketched (Ga: purple spheres, I: green spheres), and the glass composition is indicated as a dashed orange line. (B) DSC on glassy $Ga_2I_{3.17}$. Heating/cooling curves of the air-quenched glass exhibiting a glass transition at T_g = 60 °C and onset of crystallization at $T_c \approx 90$ °C. Inset: photographs of a $Ga_2I_{3.17}$ sample in a glassy (g) or crystallized (c) state at room temperature and in a liquid (l) state at 400 °C. (C) Curves (1,2): heating and subsequent cooling of an air-quenched sample; (3,4): subsequent second heating/cooling cycle; (5,6): heating/cooling curves after sub-T_g annealing (50 °C, 1 h). All curves were recorded at a rate of 10 K min^{-1}.

of Ga^+ cations and GaI_4^- or $Ga_2I_6^{2-}$ anions, respectively, which are isostructural and isoelectronic to the above-mentioned PS_4^{3-} and $P_2S_6^{4-}$ anions. The initially reported monoiodide GaI appears to correspond to the formula Ga_2I_3.[35,37] Besides the high-temperature reaction of the elements, the higher iodides can be prepared by sonicating liquid gallium metal in a solution of iodine in benzene.[38] For a 1:1 ratio of Ga/I, this yields a gray-greenish powder, which appears to be a mixture of

the above phases and has found use as a gallium source in organic synthesis.[39,40]

Two early reports noted a possible glass formation in the Ga−I system without providing further details.[37,41] Our study is the first investigation of the gallium halide glass with the composition $Ga_2I_{3.17}$, describing the local structure and chemical properties of the liquid and glassy states in detail. The reported structures of the crystalline phases, c-Ga_2I_3 and c-Ga_2I_4, were taken as starting points for the analysis of glassy and liquid $Ga_2I_{3.17}$. The crystalline compounds contain gallium in nominal oxidation states Ga(I), Ga(II), and Ga(III). In c-Ga_2I_3 and c-Ga_2I_4, Ga(I) cations coordinate with $Ga(II)_2I_6^{2-}$ heteroethane ions (idealized point symmetry D_{3d}) and tetrahedral $Ga(III)I_4^-$ anions, respectively (cf. Figure 1A). The reported covalent bond lengths in the molecular anions are 2.39 Å for the Ga(II)−Ga(II) single bond and 2.54−2.61 Å for Ga(I)−I bonds.

EXPERIMENTAL METHODS

Gallium iodide samples were prepared in a highly exothermic reaction by carefully heating stoichiometric amounts of gallium metal (Aldrich, 99.99%) and iodine powder (VWR Rectapur GPR, ≥99%) up to 300 °C, forming a dark red melt. Samples of the gallium iodide glass were prepared by air quenching a melt of composition $Ga_2I_{3.17}$ (i.e. $Ga_{38.7}I_{61.3}$), from 400 °C to room temperature. This composition corresponds to the solubility limit of Ga in the melt at 400 °C. The composition of the glass was determined as $Ga_2I_{3.17}$ by back-weighing the residual Ga metal from samples with Ga metal excess. Differential scanning calorimetry (DSC) data were collected on a PerkinElmer DSC 8000 system at a rate of 10 K min^{-1}. Raman and Fourier transform infrared (FTIR) spectra were recorded under an inert atmosphere on a Renishaw Ramascope (HeNe laser, 633 nm) and a Bruker INVENIO-R spectrometer, respectively. Time-of-flight neutron diffraction data were recorded on the GEM instrument (RAL-ISIS, UK) in the range Q = 0.1−60 Å^{-1}. The DC conductivity and AC admittance data were recorded in a two-probe mode using a UNI-T 61C ohmmeter and an Agilent HP 4294A precision impedance analyzer, respectively. Further experimental details and data evaluation are provided in the Supporting Information.

RESULTS AND DISCUSSION

During the preparation of glassy g-$Ga_2I_{3.17}$, a remarkable color change was observed from the yellow crystalline solid to a dark red liquid, which then gives an optically transparent orange glass g-$Ga_2I_{3.17}$ upon quenching (inset to Figure 1B). The glassy nature of g-$Ga_2I_{3.17}$ was confirmed by DSC of glassy $Ga_2I_{3.17}$. Heating of the air-quenched glass reveals a glass transition at T_g = 60.0 °C with a kinetic overshoot followed by a strong exothermic crystallization of the glass with onset at $T_c \approx 90$ °C at 10 K min^{-1} (Figure 1B). The glass transition displays a step in specific heat ΔC_p = 83.5 J K^{-1} mol$_{Ga2I3.17}^{-1}$ (curve 1 in Figure 1C). The glass-transition temperature was found as T_g = 57.7 °C in the second heating cycle after cooling the sample at a rate of 10 K min^{-1} (curve 3 in Figure 1C). The strong kinetic overshoot observed in the air-quenched material indicates a more relaxed sample which was reduced in the second heating cycle, suggesting that the cooling rate of the air-quenched material was significantly lower due to the large thermal mass. Sub-T_g annealing of the sample for 1 h at 50 °C led to the recovery of the kinetic overshoot and a glass transition with T_g = 60.0 °C and ΔC_p = 83.8 J K^{-1} mol$_{Ga2I3.17}^{-1}$ (curve 5 in Figure 1C).

The temperature-dependent Raman spectra of g-$Ga_2I_{3.17}$ were recorded to determine the molecular make-up of the

glass and follow the structural changes upon heating from room temperature to 410 °C, covering the glassy, supercooled liquid, crystalline, and liquid states (Figure 2). The reported
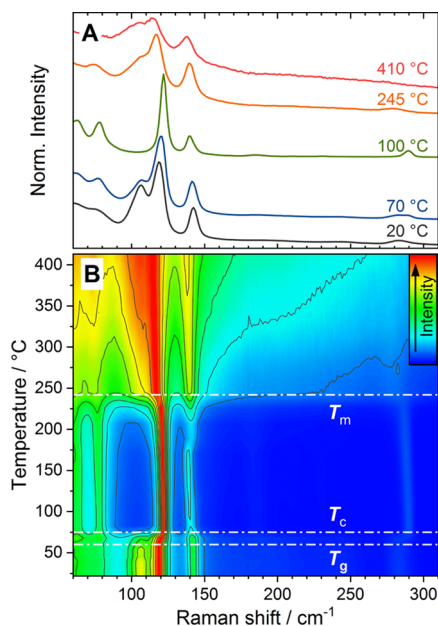

Figure 2. Raman spectra of glassy $Ga_2I_{3.17}$ recorded upon heating from room temperature to 410 °C. (A) Raman spectra at selected temperatures. Curves shifted vertically for clarity. (B) Contour plot of temperature-dependent measurements. The temperatures of glass transition T_g, crystallization T_c, and complete melting T_m are indicated by dash-dotted lines. Intensity is indicated by the color scale and contour lines. Spectra are normalized to the highest intensity.

crystal structures and Raman spectra of Ga_2I_3, Ga_2I_4, and a series of $A_2[Ga_2X_6]$ compounds, together with the calculated Raman spectrum of c-Ga_2I_3, serve as a starting point for assigning the Raman lines to the molecular modes (cf. Table S1 in the Supporting Information).[37,43,44] The composition of the melt and the resulting glass, $Ga_2I_{3.17}$, lies between that of c-Ga_2I_3 and c-Ga_2I_4, suggesting a mixture of Ga^+ ions with both $Ga_2I_6^{2-}$ and GaI_4^- molecular ions in the glass.

The Raman spectrum of g-$Ga_2I_{3.17}$ at 20 °C displays four distinct peaks centered at 106, 118, 142, and 283 cm^{-1} (Figure 2A). Modes below 80 cm^{-1} can be assigned to I–Ga–I and I–Ga–Ga bending modes of GaI_4^- and $Ga_2I_6^{2-}$ molecules, respectively. Upon close inspection, two very weak broadened features are found at 184 and 244 cm^{-1} due to the Ga–I asymmetric stretch vibrations of $Ga_2I_6^{2-}$.[43,44] The peaks at 118 and 283 cm^{-1} can be identified as the in-phase (A_{1g}) and out-of-phase (A_{1g}) stretch vibrations of the Ga–Ga bond within the $Ga_2I_6^{2-}$ ions, as observed in $A_2[Ga_2I_6]$ (A = H^+, Me_4N^+) compounds and the calculated Raman spectrum for c-Ga_2I_3 (Table S1). The peak at 142 cm^{-1} can be assigned to the tetrahedral breathing mode (A_1) of GaI_4^- molecules, the band of the highest intensity in Ga_2I_4 (cf. Figure S1 in the Supporting Information).[37] The presence of GaI_4^- molecules is consistent with the determined sample composition of $Ga_2I_{3.17}$, which corresponds to an approximate ratio of 0.4 GaI_4^- molecules per $Ga_2I_6^{2-}$ molecule. Following this analysis, the overall composition of g-$Ga_2I_{3.17}$ can also be represented as $[Ga^+]_{63.2}[Ga_2I_6^{2-}]_{26.3}[GaI_4^-]_{10.5}$, reflecting the molecular makeup.

At 106 cm^{-1}, a strong mode is observed in glassy $Ga_2I_{3.17}$ which cannot be attributed to any molecular mode of $Ga_2I_6^{2-}$ or GaI_4^- units and therefore requires further examination. The peak is of comparable intensity and width to the identified molecular modes, suggesting a localized nature (20 °C curve in Figure 2A). The mode was not observed in the infrared spectra of g-$Ga_2I_{3.17}$ (Figure S2) and hence is only Raman-active.

Two phenomena are observed for (i) the molecular modes of $Ga_2I_6^{2-}$ and GaI_4^- and (ii) the unidentified mode at 106 cm^{-1} upon heating:

(i) The Raman shift and peak width for the Ga–Ga stretch modes at 118 and 283 cm^{-1} and the GaI_4^- tetrahedral symmetric breathing mode at 142 cm^{-1} show a remarkable temperature dependence (cf. Figure S3). All three modes display an overall red shift with increasing temperature, as expected for the thermal expansion behavior of an anharmonic oscillator. Across the glass transition around 60 °C, both the Ga–Ga stretch modes of the $Ga_2I_6^{2-}$ unit experience a rapid but continuous blue shift which stops once the sample crystallizes at around 80 °C.

Contrarily, the GaI_4^- breathing mode at 142 cm^{-1} displays a red shift, simultaneous with the above-mentioned blue shift. The opposite behavior in Raman shift agrees well with the separation of $Ga_2I_6^{2-}$ and GaI_4^- molecules due to the crystallization of g-$Ga_2I_{3.17}$ forming the phases c-Ga_2I_3 and c-Ga_2I_4. During melting of the two phases, which begins for c-Ga_2I_4 at 170 °C and for c-Ga_2I_3 around 230 °C (cf. Figures 2 and S3), the change in Raman shift is reversed for all three modes.

Extrapolation of the peak positions from the glassy state to higher temperatures coincides well with the observed peak positions in the liquid state, suggesting that the interactions in glass and liquid are of similar nature. The changing line widths of all three modes reflect the narrowing and broadening distributions of the coordination environments for $Ga_2I_6^{2-}$ and GaI_4^- molecules upon crystallization and melting, respectively.

(ii) Approaching T_g, the peak at 106 cm^{-1} drastically loses intensity and is completely absent once the sample crystallizes at T_c (100 °C curve in Figure 2A). Upon melting, the peak reappears as a broad shoulder and gains intensity as the temperature increases (curves for 245 and 410 °C in Figure 2A). The mode is only present in the disordered glassy and liquid states, which contain both $Ga_2I_6^{2-}$ and GaI_4^- molecules but not after crystallization when the two types of molecules are separated in two phases. Heating of g-$Ga_2I_{3.17}$ from room temperature across T_g and subsequent cooling, while avoiding crystallization, reveal the reversibility of the intensity loss across T_g. The intensity of the 106 cm^{-1} peak drops steeply above 60 °C, relative to the highest intensity Ga–Ga stretch mode at 118 cm^{-1}, but regains nearly full initial intensity upon cooling (cf. Figure S4).

The amorphous nature of the material was further corroborated by time-of-flight neutron measurements recorded on glassy (30 °C) and liquid (310 and 400 °C) $Ga_2I_{3.17}$ (GEM diffractometer, RAL-ISIS, UK).[45] The total structure factor $S(Q)$ for glassy $Ga_2I_{3.17}$, presented as a function of the scattering vector Q in Figure 3A, shows broadened features characteristic of amorphous materials and is dominated by three main peaks in the low-Q region (Table S2). A small but well-defined first sharp diffraction peak (FSDP) is observed at $Q_1 = 0.96$ $Å^{-1}$. The FSDP can be related to intermediate-range order (IRO) on the length scale of $2\pi/Q_1 \approx 6.5$ Å. In c-Ga_2I_3, no intramolecular correlations exist beyond this length scale,
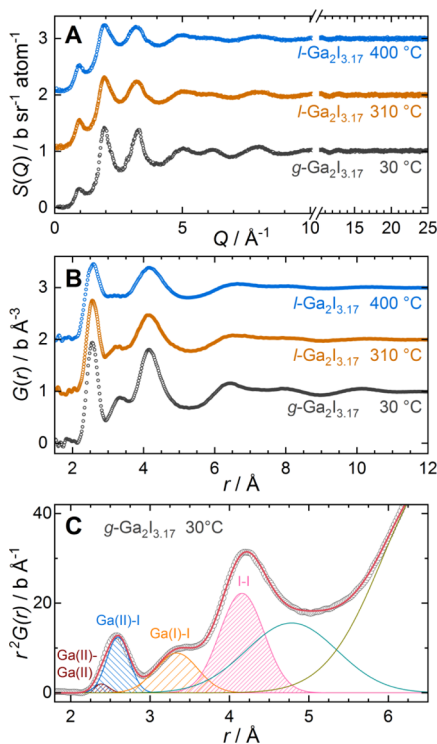
Figure 3. Neutron diffraction data for $Ga_2I_{3.17}$ in the glassy (30 °C) and liquid (310, 400 °C) states. Data are vertically shifted for visibility. (A) Total structure factors $S(Q)$ after the correction of raw data. (B) Pair distribution functions $G(r)$ obtained by Fourier transformation of the diffraction data. (C) Gaussian least-squares fit to the function $r^2G(r)$ for glassy $Ga_2I_{3.17}$. Peaks are labeled with atom pair assignments.

marking the transition to purely intermolecular pair correlations.[46,47] Comparing $S(Q)$ of g-$Ga_2I_{3.17}$ with the liquid state, an overall broadening of the features is observed at higher temperatures. Interestingly, the positions of the first and second peaks barely change upon melting, and the FSDP is sharpened, suggesting enhanced IRO. The oscillations of $S(Q)$ at high Q are dampened more strongly at high temperatures, as expected, due to thermal broadening.

The total pair distribution function $G(r)$ for glassy and liquid $Ga_2I_{3.17}$ (Figure 3B) was obtained by Fourier transformation of the total structure factor. The close correspondence of $G(r)$ for g-$Ga_2I_{3.17}$, l-$Ga_2I_{3.17}$, and c-Ga_2I_3 (cf. Figure S6) corroborates the suspected presence of $Ga_2I_6^{2-}$ molecules in glassy and liquid $Ga_2I_{3.17}$. Below $r = 2$ Å, $G(r)$ of g-$Ga_2I_{3.17}$ shows small irregular oscillations around zero, attributed to Fourier truncation artifacts, and no contributions to $G(r)$ are expected in this range. A comparison with interatomic distances observed in crystalline gallium iodides and the simulated total pair distribution function for crystalline Ga_2I_3 (Figure S6) allows the assignment of the peaks in $G(r)$ to interatomic distances between atom pairs up to $r = 5$ Å (Figure 3B,C).[37,48]

The first peak centered around 2.56 Å contains overlapping contributions of the covalently bound Ga(II)−Ga(II) (~2.39 Å) pair in $Ga_2I_6^{2-}$ and Ga−I pairs within $Ga_2I_6^{2-}$ and GaI_4^- molecules (~2.5−2.6 Å). The contribution of the Ga−Ga pairs to $G(r)$ is quite small due to the high relative abundance of Ga−I bonds and the smaller neutron scattering length of gallium. The third peak in $G(r)$ shows a maximum at $r = 4.14$ Å in good agreement with the longer nonbonded Ga(II)−

iodine distances within $Ga_2I_6^{2-}$ (~4.1 Å) and intramolecular iodine−iodine (4.2−4.3 Å, geminal) distances within the $Ga_2I_6^{2-}$ and GaI_4^- units. The asymmetry at high r arises from intramolecular I−I (vicinal) and also intermolecular I−I distances between neighboring molecules, contributing between $r = 4.1$ and 4.5 Å in the crystalline compounds.[37] The second peak centered at 3.30 Å can then be assigned to the distances between iodine in the $Ga_2I_6^{2-}$/GaI_4^- units and the surrounding Ga(I) ions, as observed in c-Ga_2I_3 and c-Ga_2I_4 ($d_{Ga(I)-I} \approx 3.3-3.7$ Å). This distribution is significantly broader than the intramolecular contributions as a result of the relaxed bonding constraints. The Ga(I)−I distribution is also significantly broadened compared to the simulated $G(r)$ of c-Ga_2I_3 (Figure S6).

For the liquid l-$Ga_2I_{3.17}$, at 310 and 400 °C, $G(r)$ shows a similar overall shape as for g-$Ga_2I_{3.17}$. Upon melting, the first and third peaks in $G(r)$ are slightly broadened, which is enhanced at 400 °C. Overall, the magnitude of the oscillations in $G(r)$ at larger distances decays faster with increasing temperature. The strongest change is observed for the second peak, around 3.3 Å. While this peak is well defined in the glassy solid, it is significantly broadened in the melt at 310 °C and turns into a nearly flat contribution to $G(r)$ at 400 °C. This observation can be well reconciled with the above peak assignment, distinguishing intramolecular Ga(II)−Ga(II) (2.39 Å), Ga(II/III)−I (2.59 Å), and I−I (4.1 Å) distances from the intermolecular Ga(I)−I distances. While the intramolecular distances show only moderate peak broadening upon melting, the distribution of the noncovalently bound Ga(I)−I pairs around $r = 3.3$ Å is strongly affected, suggesting enhanced mobility and disorder of the Ga(I) ions.

The partial coordination numbers $CN_{Ga(II)}^{Ga(II)}$, $CN_{Ga(II,III)}^I$, $CN_{Ga(I)}^I$, and CN_I^I for the peaks up to $r = 5$ Å were determined following the formalism derived in the Supporting Information. The fit results from Gaussian contributions to $r^2G(r)$ (Figures 3C and S7) were weighted by the corresponding stoichiometric coefficients and neutron scattering lengths to obtain an estimate for the partial coordination numbers (Tables 1, S3, and S4).

Table 1. Results of the Least-Squares Fit of Gaussian Contributions to the Function $r^2G(r)$ and Coordination Numbers CN_i^j of Atoms j Around i in g-$Ga_2I_{3.17}$ at 30 °C in the Range $r = 2-5$ Å

atom pair $i-j$	r/Å	fwhm/Å	area/b Å^{-2}	CN_i^j
Ga(II)−Ga(II)	2.388[a]	0.19(1)	0.47(5)	0.65(6)
Ga(II/III)−I	2.597[a]	0.284(4)	4.42(7)	3.49(6)
Ga(I)−I	3.336(8)	0.53(1)	5.9(4)	4.7(3)
I−I	4.157(2)	0.56(2)	15.6(17)	10.7(1.1)

[a]Peak position fixed to reported bond lengths in c-Ga_2I_3. Estimated standard deviations from the least-squares fit are given in brackets.

Coordination numbers for gallium in $Ga(II)_2I_6^{2-}$ or $Ga(III)I_4^-$ units by Ga(II) and iodine were obtained as $CN_{Ga(II)}^{Ga(II)} = 0.65(6)$ and $CN_{Ga(II/III)}^I = 3.49(6)$, respectively. The individual and summed coordination numbers agree closely with the expected values for tetrahedrally coordinated gallium in a mixture of both $Ga_2I_6^{2-}$ (ideal: $CN_{Ga(II)}^{Ga(II)} = 1$ and $CN_{Ga(II)}^I = 3$) and GaI_4^- (ideal: $CN_{Ga(III)}^I = 4$) molecular anions, considering the strong overlap of both peaks. The average coordination number of the individual Ga(I) cations (i.e., Ga$^+$) by iodine $CN_{Ga(I)}^I = 4.7(3)$ is significantly reduced in glassy

$Ga_2I_{3.17}$ compared to crystalline Ga_2I_3, where eight iodine atoms form the closest coordination shell. Upon melting, the distribution broadens, and $CN^I_{Ga(I)}$ decreases to 4.2(1) at 400 °C (Tables S3 and S4). At a higher temperature and above r = 4 Å, the coordination numbers are less robust due to the increased overlap of partial contributions and the simplistic approximation as symmetric Gaussian contributions.

The effect of structural changes on the transport properties of $Ga_2I_{3.17}$ was observed in the temperature-dependent measurements of electrical dc conductivity and ac admittance spectra. The DC conductivity $\sigma(T)$ of g-$Ga_2I_{3.17}$ was measured as a function of temperature while the sample was heated from room temperature through the glass transition and subsequent crystallization. The dc conductivity changes by several orders of magnitude as it passes through three distinct stages, delimited by the glass-transition temperature T_g and the crystallization temperature T_c (Figure 4A). Below T_g, g-$Ga_2I_{3.17}$ displays a linear trend of $\ln(\sigma)$ versus $1/T$, suggesting a thermally activated process for the mobility of Ga(I) ions. The behavior is well described by the Arrhenius law $\sigma(T)$ =

Figure 4. (A) Electrical dc conductivity measured upon heating of a g-$Ga_2I_{3.17}$ sample. Fit functions and parameters for three regions (T < T_g, T_g < T < T_c, T_c < T). (B) Real part $Y_{Re}(\omega)$ and (C) imaginary part $-Y_{im}(\omega)$ of the ac admittance for glassy $Ga_2I_{3.17}$. Inset to (B): Extrapolated low-frequency limit $Y_{Re}(\omega = 0)$. Arrows in (C) are guide to the eye, highlighting the approximate temperature dependence of the characteristic frequencies for the three suggested relaxation processes.

$\sigma_0 e^{-E_a/kT}$, with the fit parameters σ_0 = 156.6 S cm^{-1} and the activation energy E_a = 0.59 eV.

Above the glass transition, which has a lower onset than in DSC due to the lower heating rate, $\ln[\sigma(T)]$ deviates strongly from the linear behavior, that is, from exponential relaxation, and increases at an accelerated rate. Such behavior is typically observed for glass systems containing mobile ionic species and indicates the onset of a cooperative mechanism for the conduction of Ga(I) ions as $Ga_2I_6^{2-}$, and GaI_4^- units gain structural freedom.[49] Conductivity enhancement due to a cooperative mechanism was recently also reported for the molecular glass Li_3PS_4.[28] The supercooled liquid region T_g < T < T_c can be well fitted using the empirical Vogel−Fulcher− Tammann (VFT) expression $\sigma(T)$ = $\sigma_{VFT} e^{-E_{VFT}/k(T-T_0)}$.[50] This yields the fit parameters E_{VFT} = 0.014 eV, T_0 = 296 K, and σ_{VFT} = 1.36 10^{-4} S cm^{-1}.

The real part $Y_{Re}(\omega)$ of the spectral ac admittance (i.e., the inverse of the complex electrical impedance) in the glassy state presents a wide low-frequency plateau, extending to higher frequencies as the ionic mobility increases with temperature (Figure 4B). This corresponds to the bulk ionic conductivity, and the extrapolated values $Y_{Re}(\omega = 0)$ (inset to Figure 4B) follow the observed increase in the dc conductivity of g-$Ga_2I_{3.17}$, reproducing a comparable activation energy of 0.8 eV below T_g. A high-frequency limit is not observed within the recorded range (40 Hz − 50 MHz), as data above 3 MHz are influenced by the strong pickup from wiring contributions.[51]

The respective imaginary part $-Y_{im}(\omega)$ of ac admittance is characterized by a broad minimum centered around $\omega_{mean} \approx$ 10^4 Hz at 23 °C (Figure 4C). With increasing temperature, the relaxation time decreases and the broad minimum splits into two individual contributions around $T_g \approx$ 37–41 °C, before ending in a single narrow minimum at 0.5−1.4 × 10^6 Hz above 44 °C, indicating a single relaxation process.[52]

The clear observation of two relaxation processes around T_g with distinct time constants is intriguing and raises questions about their structural origins.[53] In amorphous polymers and glass-forming liquids, the primary or structural α-relaxation determines the glass transition and has been related to cooperative molecular rearrangements.[54,55] For many materials, a secondary β-relaxation, or Johari−Goldstein relaxation, has been observed in their dielectric or impedance spectra, which manifests as a high-frequency contribution on an individual timescale and temperature dependence.[56] Its exact nature is still debated but has been associated with hindered noncooperative reorientations or translations in the local regions of low mobility.[57]

Within this model, the two observed minima may be attributed to the above-described structural primary and secondary β-relaxation.[58] The timescale of the primary relaxation is observable as a low-frequency contribution close to the glass-transition temperature but is indistinguishable from the β-relaxation above T_g. The exact temperature dependence of the low-frequency contribution is hard to determine within the narrow observation window.

The narrowing of the minimum at low temperatures may be attributed to the freeze-out and decrease in magnitude of the primary relaxation mechanism. Thus, the primary relaxation may be understood as cooperative translations and reorientations of Ga(I), $Ga_2I_6^{2-}$, and GaI_4^- ions in g-$Ga_2I_{3.17}$.

Below T_g, the movement of molecular units freezes out, and the Ga(I) migration follows pure Arrhenius behavior.[59] A third contribution, corresponding to the slow time constant of the
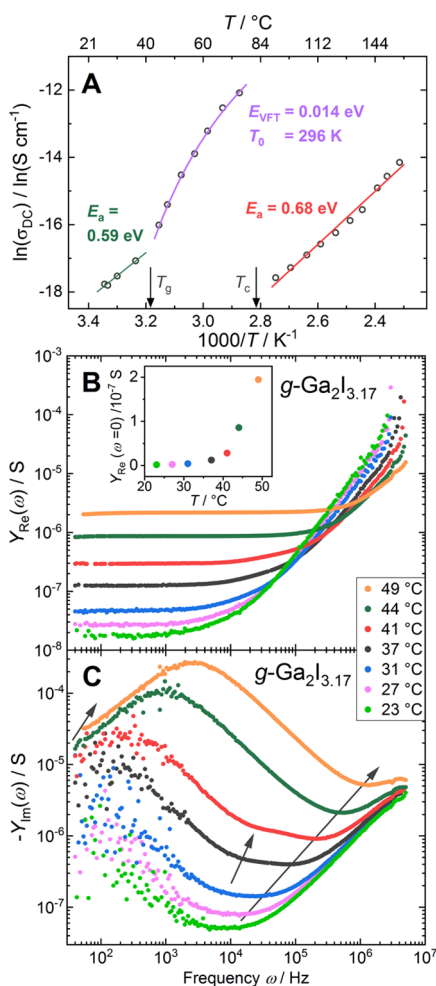
electrode/electrolyte contact, gives rise to a minimum at low frequencies ($\omega < 10^2$ Hz), which is not resolved within the observed frequency range.

As the sample crystallizes into a physical mixture of c-Ga_2I_3 and c-Ga_2I_4 around 80 °C, the dc conductivity drops by 2 orders of magnitude, and the Arrhenius behavior is restored. A linear fit to $\ln(\sigma)$ versus $1/T$ yields an activation energy of $E_a = 0.68$ eV, corresponding to a 15% increase compared to that of g-$Ga_2I_{3.17}$ ($E_a = 0.59$ eV). While the two-phase nature of the crystalline sample complicates interpretation, the increased energy barrier for Ga(I) migration is in line with the change in the average coordination number of Ga(I) by iodine from 4.6 in g-$Ga_2I_{3.17}$ to 8 in c-Ga_2I_3 and c-Ga_2I_4, as observed in neutron diffraction. A comparable value for the activation enthalpy of 0.8 eV has been reported for the electrical conductivity of the structurally related crystalline compound Ga_2Br_3.[60] High ionic conductivity appears as a universal property of the $A_2[Ga_2X_6]$-related compounds, rendering especially the lithium analogues interesting for application.[48] The electrical ac admittance in the crystallized sample displays a low-frequency plateau in $Y_{Re}(\omega)$ in line with the observed ionic dc conductivity, and $-Y_{im}(\omega)$ indicates a single relaxation mechanism (Figure S8).

CONCLUSIONS

A high glass-forming tendency was found for melts with composition $Ga_2I_{3.17}$, located between the two binary crystalline compounds Ga_2I_3 and Ga_2I_4. Raman spectroscopy and neutron scattering revealed that the $Ga_2I_{3.17}$ glass can be described as a mixture of the molecular anions $Ga_2I_6^{2-}$ and GaI_4^- coordinated by Ga^+ cations. Remarkably, the glass contains gallium in three formal oxidation states, and its molecular make-up can be summarized by the formula $[Ga^+]_{63.2}[Ga_2I_6^{2-}]_{26.3}[GaI_4^-]_{10.5}$.

A strong Raman mode at 106 cm^{-1} was observed for glassy and liquid $Ga_2I_{3.17}$, which is absent in the spectra of the crystalline phases Ga_2I_3 and Ga_2I_4 and indicative of strong intermolecular interactions at the glass composition. Temperature-dependent Raman and admittance spectroscopy show that the new mode is strongly connected to the local structure in glassy and liquid $Ga_2I_{3.17}$ and the structural relaxation at the glass transition. The sharp peak shape suggests the resonance of a well-defined local molecular arrangement possible only in the presence of both $Ga_2I_6^{2-}$ and GaI_4^- units.

Comparison of the extrapolated dc conductivity of the crystallized mixture Ga_2I_3/Ga_2I_4 suggests a conductivity increase by several orders of magnitude in glassy $Ga_2I_{3.17}$ compared to the ordered crystalline phases. The existence of the related crystalline compounds $LiGaI_3$, $LiGaBr_3$, and $LiGaCl_3$[48,61] hints that g-$Ga_2I_{3.17}$ may be the first representative of a whole family of mixed molecular glasses with substitutional flexibility, heralding the advent of new ion-conducting glasses for lithium- or sodium-based energy storage concepts.

ASSOCIATED CONTENT

Supporting Information

The Supporting Information is available free of charge at https://pubs.acs.org/doi/10.1021/acs.inorgchem.1c00049.

Full experimental details on synthesis, characterization, and evaluation of neutron diffraction data; detailed Raman, infrared, and neutron diffraction data; Raman/infrared modes; and results of neutron diffraction data (PDF)

AUTHOR INFORMATION

Corresponding Author

Alfred Amon − Department of Chemistry, University College London, WC1H 0AJ London, U.K.; orcid.org/0000-0002-5301-8867; Email: a.amon@ucl.ac.uk

Authors

M. Emre Sener − Department of Chemistry, University College London, WC1H 0AJ London, U.K.

Alexander Rosu-Finsen − Department of Chemistry, University College London, WC1H 0AJ London, U.K.; orcid.org/0000-0001-5165-7940

Alex C. Hannon − ISIS Facility, Rutherford Appleton Laboratory, OX11 0QX Didcot, U.K.; orcid.org/0000-0001-5914-1295

Ben Slater − Department of Chemistry, University College London, WC1H 0AJ London, U.K.

Christoph G. Salzmann − Department of Chemistry, University College London, WC1H 0AJ London, U.K.; orcid.org/0000-0002-0714-7342

Complete contact information is available at:
https://pubs.acs.org/10.1021/acs.inorgchem.1c00049

Author Contributions

A.A. wrote the manuscript and performed DSC, Raman, FTIR, conductivity, and neutron diffraction experiments. M.E.S. performed conductivity measurements, optical spectroscopy, and data evaluation. A.R.-S. and A.C.H. performed neutron diffraction measurements. B.S. performed computational analyses. A.A. and C.G.S. developed the concept of this study. All authors have given approval to the final version of the manuscript.

Notes

The authors declare no competing financial interest.

ACKNOWLEDGMENTS

REFERENCES

(1) Martin, B.; Weaver, J. C. Materials Science and Architecture. *Nat. Rev. Mater.* **2017**, 2, 17082.

(2) Frankberg, E. J.; Kalikka, J.; García Ferré, F.; Joly-Pottuz, L.; Salminen, T.; Hintikka, J.; Hokka, M.; Koneti, S.; Douillard, T.; Le Saint, B.; Kreiml, P.; Cordill, M. J.; Epicier, T.; Stauffer, D.; Vanazzi, M.; Roiban, L.; Akola, J.; Di Fonzo, F.; Levänen, E.; Masenelli-Varlot, K. Highly Ductile Amorphous Oxide at Room Temperature and High Strain Rate. *Science* **2019**, 366, 864−869.

(3) Wuttig, M.; Yamada, N. Phase-Change Materials for Rewriteable Data Storage. *Nat. Mater.* **2007**, 6, 824−832.

(4) Chen, M. A Brief Overview of Bulk Metallic Glasses. *NPG Asia Mater.* **2011**, 3, 82−90.

(5) Bennett, T. D.; Tan, J.-C.; Yue, Y.; Baxter, E.; Ducati, C.; Terrill, N. J.; Yeung, H. H.-M.; Zhou, Z.; Chen, W.; Henke, S.; Cheetham, A.

K.; Greaves, G. N. Hybrid Glasses from Strong and Fragile Metal-Organic Framework Liquids. *Nat. Commun.* **2015**, *6*, 8079.

(6) Qiao, A.; Bennett, T. D.; Tao, H.; Krajnc, A.; Mali, G.; Doherty, C. M.; Thornton, A. W.; Mauro, J. C.; Greaves, G. N.; Yue, Y. A Metal-Organic Framework with Ultrahigh Glass-Forming Ability. *Sci. Adv.* **2018**, *4*, No. eaao6827.

(7) Cao, C.; Li, Z.-B.; Wang, X.-L.; Zhao, X.-B.; Han, W.-Q. Recent Advances in Inorganic Solid Electrolytes for Lithium Batteries. *Front. Energy Res.* **2014**, *2*, 25.

(8) Kraft, M. A.; Ohno, S.; Zinkevich, T.; Koerver, R.; Culver, S. P.; Fuchs, T.; Senyshyn, A.; Indris, S.; Morgan, B. J.; Zeier, W. G. Inducing High Ionic Conductivity in the Lithium Superionic Argyrodites $Li_{6+x}P_{1-x}Ge_xS_5I$ for All-Solid-State Batteries. *J. Am. Chem. Soc.* **2018**, *140*, 16330−16339.

(9) Pavic, L.; Sklepić, K.; Skoko, Ž.; Tricot, G.; Mošner, P.; Koudelka, L.; Moguš-Milanković, A. Ionic Conductivity of Lithium Germanium Phosphate Glass-Ceramics. *J. Phys. Chem. C* **2019**, *123*, 23312−23322.

(10) Yamanaka, T.; Hayashi, A.; Yamauchi, A.; Tatsumisago, M. Preparation of Magnesium Ion Conducting $MgS–P_2S_5–MgI_2$ Glasses by a Mechanochemical Technique. *Solid State Ionics* **2014**, *262*, 601−603.

(11) Ping, W.; Paraska, D.; Baker, R.; Harrowell, P.; Angell, C. A. Molecular Engineering of the Glass Transition: Glass-Forming Ability across a Homologous Series of Cyclic Stilbenes. *J. Phys. Chem. B* **2011**, *115*, 4696−4702.

(12) Plante, A.; Palato, S.; Lebel, O.; Soldera, A. Functionalization of Molecular Glasses: Effect on the Glass Transition Temperature. *J. Mater. Chem. C* **2013**, *1*, 1037−1042.

(13) Shirota, Y. Photo- and electroactive amorphous molecular materials-molecular design, syntheses, reactions, properties, and applications. *J. Mater. Chem.* **2005**, *15*, 75−93.

(14) Strohriegl, P.; Grazulevicius, J. V. Charge-Transporting Molecular Glasses. *Adv. Mater.* **2002**, *14*, 1439−1452.

(15) Gujral, A.; Yu, L.; Ediger, M. D. Anisotropic Organic Glasses. *Curr. Opin. Solid State Mater. Sci.* **2018**, *22*, 49−57.

(16) Yu, L. Amorphous Pharmaceutical Solids: Preparation, Characterization and Stabilization. *Adv. Drug Deliv. Rev.* **2001**, *48*, 27−42.

(17) Kawakami, K.; Harada, T.; Yoshihashi, Y.; Yonemochi, E.; Terada, K.; Moriyama, H. Correlation between Glass-Forming Ability and Fragility of Pharmaceutical Compounds. *J. Phys. Chem. B* **2015**, *119*, 4873−4880.

(18) Liu, G.; Li, A.-Y.; An, D.; Wu, H.-B.; Zhu, X.-H.; Li, Y.; Miao, X.-R.; Deng, W.-L.; Yang, W.; Cao, Y.; Roncali, J. An Ionic Molecular Glass as Electron Injection Layer for Efficient Polymer Light-Emitting Diode. *Macromol. Rapid Commun.* **2009**, *30*, 1484−1491.

(19) Naito, K. Quantitative Relations between Glass Transition Temperatures and Thermodynamic Parameters for Various Materials: Molecular Design for Nonpolymeric Organic Dye Glasses with Thermal Stability. *Chem. Mater.* **1994**, *6*, 2343−2350.

(20) Lebel, O.; Maris, T.; Perron, M.-È.; Demers, E.; Wuest, J. D. The Dark Side of Crystal Engineering: Creating Glasses from Small Symmetric Molecules That Form Multiple Hydrogen Bonds. *J. Am. Chem. Soc.* **2006**, *128*, 10372−10373.

(21) Kinoshita, M.; Kita, H.; Shirota, Y. A Novel Family of Boron-Containing Hole-Blocking Amorphous Molecular Materials for Blue- and Blue-Violet-Emitting Organic Electroluminescent Devices. *Adv. Funct. Mater.* **2002**, *12*, 780−786.

(22) Boils, D.; Perron, M.-È.; Monchamp, F.; Duval, H.; Maris, T.; Wuest, J. D. Molecular Tectonics. Disruption of Self-Association in Melts Derived from Hydrogen-Bonded Solids. *Macromolecules* **2004**, *37*, 7351−7357.

(23) Hatakeyama-Sato, K.; Tezuka, T.; Umeki, M.; Oyaizu, K. AI-Assisted Exploration of Superionic Glass-Type Li^+ Conductors with Aromatic Structures. *J. Am. Chem. Soc.* **2020**, *142*, 3301−3305.

(24) Alhalaweh, A.; Alzghoul, A.; Kaialy, W.; Mahlin, D.; Bergström, C. A. S. Computational Predictions of Glass-Forming Ability and Crystallization Tendency of Drug Molecules. *Mol. Pharm.* **2014**, *11*, 3123−3132.

(25) Qiu, Y.; Antony, L. W.; Torkelson, J. M.; de Pablo, J. J.; Ediger, M. D. Tenfold Increase in the Photostability of an Azobenzene Guest in Vapor-Deposited Glass Mixtures. *J. Chem. Phys.* **2018**, *149*, 204503.

(26) Kim, S.-Y.; Jeong, W.-I.; Mayr, C.; Park, Y.-S.; Kim, K.-H.; Lee, J.-H.; Moon, C.-K.; Brütting, W.; Kim, J.-J. Organic Light-Emitting Diodes with 30% External Quantum Efficiency Based on a Horizontally Oriented Emitter. *Adv. Funct. Mater.* **2013**, *23*, 3896−3900.

(27) Greaves, G. N.; Sen, S. Inorganic Glasses, Glass-Forming Liquids and Amorphizing Solids. *Adv. Phys.* **2007**, *56*, 1−166.

(28) Smith, J. G.; Siegel, D. J. Low-Temperature Paddlewheel Effect in Glassy Solid Electrolytes. *Nat. Commun.* **2020**, *11*, 1483.

(29) Hibi, Y.; Tanibata, N.; Hayashi, A.; Tatsumisago, M. Preparation of Sodium Ion Conducting $Na_3PS_4–NaI$ Glasses by a Mechanochemical Technique. *Solid State Ionics* **2015**, *270*, 6−9.

(30) Eckert, H. Structural Characterization of Noncrystalline Solids and Glasses Using Solid State NMR. *Prog. Nucl. Magn. Reson. Spectrosc.* **1992**, *24*, 159−293.

(31) Verrall, D. J.; Elliott, S. R. Experimental Evidence for an Inorganic Molecular Glass. *Phys. Rev. Lett.* **1988**, *61*, 974−977.

(32) Brazhkin, V. V.; Gavrilyuk, A. G.; Lyapin, A. G.; Timofeev, Y. A.; Katayama, Y.; Kohara, S. AsS: Bulk Inorganic Molecular-Based Chalcogenide Glass. *Appl. Phys. Lett.* **2007**, *91*, 031912.

(33) Blachnik, R.; Lönnecke, P.; Nuß, J. Gläser Und Verbindungen Im System $P_4S_4–As_4S_4 — As_4Se_4 — P_4Se_4$ / Glass and Compounds in the System $P_4S_4–As_4S_4—As_4Se_4—P_4Se_4$. *Z. Naturforsch. B Chem. Sci.* **1993**, *48*, 1175−1180.

(34) Klemm, W.; Tilk, W. Beiträge zur Kenntnis der Verbindungen des Galliums und Indiums. V. Die Eigenschaften der Galliumtrihalogenide. *Z. Anorg. Allg. Chem.* **1932**, *207*, 161−174.

(35) Corbett, J. D.; McMullan, R. K. The Lower Oxidation States of Gallium. I. The GaI3-GaI2-GaI System*. *J. Am. Chem. Soc.* **1955**, *77*, 4217−4219.

(36) Chadwick, J. R.; Atkinson, A. W.; Huckstepp, B. G. Phase studies of the In—Cl and Ga—I systems. *J. Inorg. Nucl. Chem.* **1966**, *28*, 1021−1026.

(37) Gerlach, G.; Hönle, W.; Simon, A. Eigenschaften Und Strukturen Reduzierter Galliumiodide: Ga_2I_4 Und Ga_2I_3. *Z. Anorg. Allg. Chem.* **1982**, *486*, 7−21.

(38) Beamish, J. C.; Wilkinson, M.; Worrall, I. J. Facile Synthesis of the Lower Valent Halides of Gallium, Ga_2X_4 (X = Chloride, Bromide, Iodide) and Tetragallium Hexaiodide. *Inorg. Chem.* **1978**, *17*, 2026−2027.

(39) Baker, R. J.; Jones, C. "GaI": A Versatile Reagent for the Synthetic Chemist. *Dalton Trans.* **2005**, *8*, 1341−1348.

(40) Malbrecht, B. J.; Dube, J. W.; Willans, M. J.; Ragogna, P. J. Addressing the Chemical Sorcery of ″GaI″: Benefits of Solid-State Analysis Aiding in the Synthesis of P→Ga Coordination Compounds. *Inorg. Chem.* **2014**, *53*, 9644−9656.

(41) Riebling, E. F.; Erickson, C. E. Molten Salt System Gallium Monoiodide-gallium Triiodide. Ii. Vapor Pressures and Species1. *J. Phys. Chem.* **1963**, *67*, 509−511.

(42) Predel, B. *Phase Equilibria, Crystallographic and Thermodynamic Data of Binary Alloys*; Madelung, O., Ed.; Springer Berlin Heidelberg: Berlin, Heidelberg, 1998; Vol. *Ni-Np−Pt-Zr*, pp 1−2.

(43) Evans, C. A.; Taylor, M. J. Gallium-gallium bonds in hexahalogenodigallate(II) ions. *J. Chem. Soc. D* **1969**, *0*, 1201−1202.

(44) Evans, C. A.; Tan, K. H.; Tapper, S. P.; Taylor, M. J. Vibrational Spectra and Metal−Metal Bonding in the Hexahalogenodigallate(II) Ions, $Ga_2X_6^{2-}$(X = Cl, Br, and I). *Dalton Trans.* **1973**, *9*, 988−991.

(45) Hannon, A. C. Results on Disordered Materials from the GEneral Materials Diffractometer, GEM, at ISIS. *Nucl. Instrum. Methods Phys. Res. Sect. A Accel. Spectrom. Detect. Assoc. Equip.* **2005**, *551*, 88−107.

(46) Salmon, P. S. Real space manifestation of the first sharp diffraction peak in the structure factor of liquid and glassy materials. *Proc. R. Soc. London, Ser. A* **1994**, *445*, 351−365.

(47) Price, D L; Moss, S C; Reijers, R; Saboungi, M -L; Susman, S Intermediate-range order in glasses and liquids. *J. Phys.: Condens. Matter* **1989**, *1*, 1005−1008.

(48) Hönle, W.; Miller, G.; Simon, A. Preparation, crystal structures, and electronic properties of LiGaCl3 and LiGaI3. *J. Solid State Chem.* **1988**, *75*, 147−155.

(49) Angell, C. A. Relaxation in liquids, polymers and plastic crystals - strong/fragile patterns and problems. *J. Non-Cryst. Solids* **1991**, *131−133*, 13−31.

(50) Böhmer, R.; Ngai, K. L.; Angell, C. A.; Plazek, D. J. Nonexponential Relaxations in Strong and Fragile Glass Formers. *J. Chem. Phys.* **1993**, *99*, 4201−4209.

(51) *Impedance Spectroscopy*; Barsoukov, E., Macdonald, J. R., Eds.; Wiley, 2005.

(52) Orazem, M. E.; Tribollet, B. *Electrochemical Impedance Spectroscopy*; John Wiley & Sons, Inc., 2008.

(53) Angell, C. A.; Ngai, K. L.; McKenna, G. B.; McMillan, P. F.; Martin, S. W. Relaxation in Glassforming Liquids and Amorphous Solids. *J. Appl. Phys.* **2000**, *88*, 3113−3157.

(54) Johari, G. P.; Goldstein, M. Viscous Liquids and the Glass Transition. II. Secondary Relaxations in Glasses of Rigid Molecules. *J. Chem. Phys.* **1970**, *53*, 2372−2388.

(55) Goldstein, M. Viscous Liquids and the Glass Transition: A Potential Energy Barrier Picture. *J. Chem. Phys.* **1969**, *51*, 3728−3739.

(56) Shin, D.-M.; Choi, J.-r.; Oh, J.-W.; Kim, H. K.; Han, D.-W.; Kim, K.; Hwang, Y.-H. Exploring the Use of Impedance Spectroscopy in Relaxation and Electrochemical Studies. *Appl. Spectrosc. Rev.* **2017**, *53*, 157−176.

(57) Cummins, H. Z. Dynamics of supercooled liquids: excess wings, β peaks, and rotation-translation coupling. *J. Phys. Condens. Matter* **2005**, *17*, 1457−1470.

(58) Johari, G. P. Localized molecular motions of β-relaxation and its energy landscape. *J. Non-Cryst. Solids* **2002**, *307−310*, 317−325.

(59) Johari, G. P. Disorder, Configurational Relaxations and Heat Capacity of Glasses. *Phase Transitions* **1985**, *5*, 277−300.

(60) Hönle, W.; Gerlach, G.; Weppner, W.; Simon, A. Preparation, Crystal Structure, and Ionic Conductivity of Digallium Tribromide, Ga_2Br_3. *J. Solid State Chem.* **1986**, *61*, 171−180.

(61) Hönle, W.; Simon, A. Darstellung Und Kristallstrukturen von $LiGaBr_4$ Und $LiGaBr_3$/Preparation and Crystal Structure of $LiGaBr_4$ and $LiGaBr_3$. *Z. Naturforsch. B Chem. Sci.* **1986**, *41*, 1391−1398.